Supporting Information

Visualizing the Initial Step of Self-Assembly and the Phase Transition by Stereogenic Amphiphiles with Aggregation-Induced Emission

Hui-Qing Peng,[†,‡,#] Bin Liu,[∥,#] Peifa Wei,[†,‡] Pengfei Zhang,[†,‡] Haoke Zhang,[†,‡] Jinfeng Zhang,[⊥] Kai Li,[†,‡] Ying Li,[†,‡] Yanhua Cheng,[†,‡] Jacky W. Y. Lam,[†,‡] Wenjun Zhang,[∥] Chun-Sing Lee,[⊥] and Ben Zhong Tang[,†,‡,§]*

[†]HKUST-Shenzhen Research Institute, No. 9 Yuexing first RD, South Area, Hi-tech Park, Nanshan, Shenzhen 518057, China

[‡]Department of Chemistry, the Hong Kong Branch of Chinese National Engineering Research Center for Tissue Restoration and Reconstruction and Institute for Advanced Study, The Hong Kong University of Science and Technology, Clear Water Bay, Kowloon, Hong Kong 999077, China

[§]Center for Aggregation-Induced Emission, SCUT-HKUST Joint Research Institute, State Key Laboratory of Luminescent Materials and Devices, South China University of Technology, Guangzhou 510640, China

[∥]Center of Super-Diamond and Advanced Films (COSDAF) & Department of Materials Science and Engineering, City University of Hong Kong, Tat Chee Avenue, Kowloon, Hong Kong, China

[⊥]Center of Super-Diamond and Advanced Films (COSDAF) & Department of Chemistry, City University of Hong Kong, Tat Chee Avenue, Kowloon, Hong Kong, China

[#]H.-Q. Peng and B. Liu contributed equally to this work.

1. General Experimental Section

All reagents were purchased from commercial suppliers and used without further purification unless otherwise mentioned. NMR spectra were obtained on a Bruker Avance 400 MHz or 600 MHz spectrometer. High-resolution mass spectra were determined on a Finnigan MAT TSQ 7000 mass spectrometer operated in a MALDI-TOF mode. Absorption and transmittance experiments were performed on a Milton Roy Spectronic 3000 Array spectrophotometer. Photoluminescence spectra were obtained on a Horiba Fluorolog-3 spectrofluorometer. The phase transition behaviors of the stereoisomers were studied on a Perkin Elmer Lambda 950 UV-Visible NIR spectrometer and a Hitachi F-4500 spectrofluorometer with temperature-controlling systems. A Philips CM200 FEG transmission electron microscopy (TEM) was used to observe the formation of the micelles and vesicles. For the preparation of TEM samples, a carbon film was immerged in a solution of (*Z*)-TPE-OEG or (*E*)-TPE-OEG followed by instantly freeze the solution by liquid nitrogen and then the frozen solution was freeze-dried (Labconco freeze dryer). As a result, the samples with original morphologies of the self-assembly nanostructures was covered on the carbon film. Scanning electron microscopy was carried out on a SIRION-100 (FEI) SEM. The SEM sample was prepared by putting a silica substrate in the aqueous solution of (*Z*)-TPE-OEG and pyrene. After took the substrate out and dried it in the air, the sample was drawn by a needle tip for partial peeling off the film (Figure 3B). The sample was coated with gold nanoparticles to improve their electron conductibility for better resolution. The specific viscosity of the aqueous solution of (*Z*)-TPE-OEG (3 mM) before and after pyrene entrapment were measured by a Ubbelohde viscometer. For the visualization of the phase transition process, one tailor-made iron plate with a circular hole was used for filling the aqueous solution of (*Z*)-TPE-OEG, which was sealed in the hole with two cover glasses.

The molar ratio of pyrene self-assembled with (*Z*)-amphiphile was calculated based on the extinction coefficient (ε). First, the absorption spectra of chloroform solutions of pyrene (c = 10 μM) and (*Z*)-TPE-OEG (c = 10 μM) were measured. By the Lambert-Beer law (A = εbc, where b indicates the thickness of the sample), the extinction coefficients of (*Z*)-TPE-OEG at 360 nm and 337 nm were calculated to be 1.81 × 104 and 2.46 × 104 M-1cm-1, respectively. The extinction coefficient of pyrene at 337 nm was calculated to be 3.44 × 104 M-1cm-1. A small fraction of the aqueous solution of (*Z*)-amphiphile with pyrene entrapment (16 μL) was evaporated and the solutes were redissolved by 2 mL chloroform. The concentration of (*Z*)-TPE-OEG at this mixture was calculated to be 23.57 μM according to its ε value at 360 nm. Accordingly, the absorbance of (*Z*)-amphiphile at 337 nm should be A = 0.5798. However, the absorbance of the mixture at this wavelength is 0.8087. Thus, the absorbance of pyrene at this wavelength (337 nm) is A = 0.2289. In combination of its extinction coefficient, the concentration of pyrene is calculated to be 6.65 μM. The molar ratio of pyrene self-assembled with (*Z*)-TPE-OEG is 6.65 μM/23.57 μM = 28.2 %.

2. Synthesis and Separation

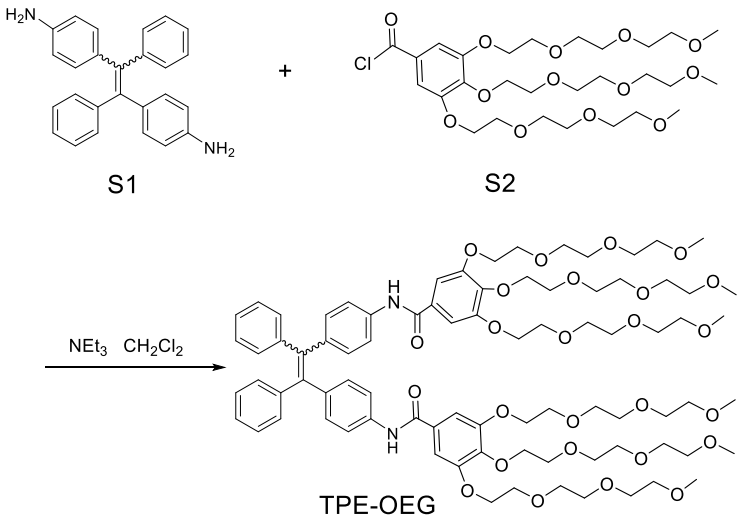

Scheme S1. Synthesis of OEG-functionalized TPE.

Triethylamine (450 μL) was added dropwise to a solution of S1[1] (362.5 mg, 1.0 mmol) and S2[2,3] (1.9 g, 3.0 mmol) in 30 mL dichloromethane. The resulting mixture was stirred at room temperature for overnight, after which the solvent was removed on a rotary evaporater. The crude product was purified by silica-gel column chromatography with 2% methanol in dichloromethane as eluent, to afford 946 mg of product. Yield: 61.3%. The isomers (*Z*)-TPE-OEG and (*E*)-TPE-OEG were separated by high-performance liquid chromatography using acetonitrile/water (7/3, v/v) as eluent. The molar ratio of the obtained (*Z*)- and (*E*)-isomers was about 1:3. Characterization for (*Z*)-TPE-OEG: ^{1}H NMR ($CDCl_3$, 400 MHz, ppm): δ 8.36 (s, 2H), 7.43 (d, J = 8.0 Hz, 4H), 7.18 (s, 4H), 7.11-7.05 (m, 10H), 7.00 (d, J = 8.0 Hz, 4H), 4.23-4.20 (m, 12H), 3.85-3.77 (m, 12H), 3.72-3.69 (m, 12H), 3.66-3.60 (m, 24H), 3.55-3.49 (m, 12H), 3.36 (s, 7H), 3.31 (s, 11H). ^{13}C NMR ($CDCl_3$, 100 MHz): δ 164.59, 151.86, 143.15, 139.61, 139.14, 136.02, 131.36, 130.81, 129.64, 127.13, 125.84, 118.71, 107.15, 71.72, 71.27, 71.24, 70.02, 69.99, 69.94, 69.89, 69.85, 69.77, 69.16, 68.54, 58.38, 58.33. HRMS: calcd for $C_{82}H_{114}N_2O_{26}$: 1542.7660; found: 1542.7694. For (*E*)-TPE-OEG: ^{1}H NMR ($CDCl_3$, 400 MHz, ppm): δ 8.38 (s, 2H), 7.45 (d, J = 8.0 Hz, 4H), 7.19 (s, 4H), 7.10-7.08 (m, 6H), 7.05-7.01 (m, 8H), 4.24-4.20 (m, 12H), 3.85-3.78 (m, 12H), 3.72-3.69 (m, 12H), 3.65-3.60 (m, 24H), 3.55-3.49 (m, 12H), 3.37 (s, 6H), 3.31 (s, 12H). ^{13}C NMR ($CDCl_3$, 100 MHz): δ 164.99, 151.64, 143.07, 140.63, 139.55, 139.08, 136.19, 131.13, 130.69, 129.38, 126.94, 125.71, 119.61, 106.67, 71.65, 71.20, 71.16, 69.95, 69.84, 69.77, 69.71, 69.00, 68.23, 58.27, 58.21. HRMS: calcd for $C_{82}H_{114}N_2O_{26}$: 1542.7660; found: 1542.7622.

3. Results and Discussion

3.1. Structure Characterizations

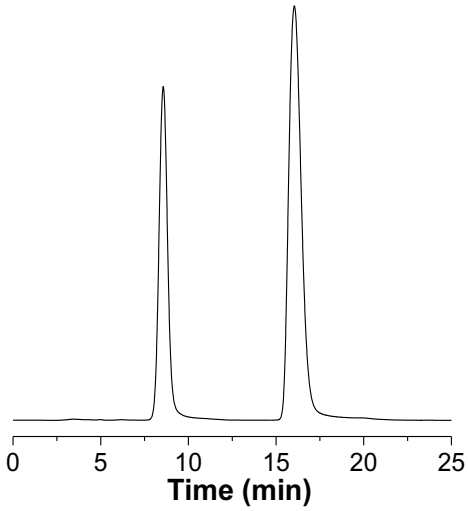

Figure S1. HPLC spectrum of (*Z*)- and (*E*)-isomers with acetonitrile/water (7:3, v/v) as eluent.

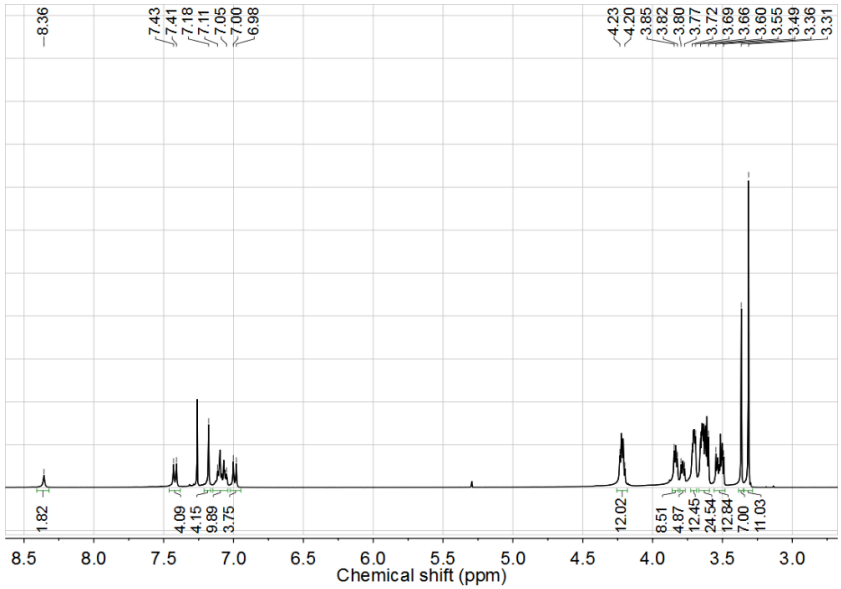

Figure S2. ^{1}H NMR spectrum of (*Z*)-TPE-OEG in $CDCl_3$ (500 μL).

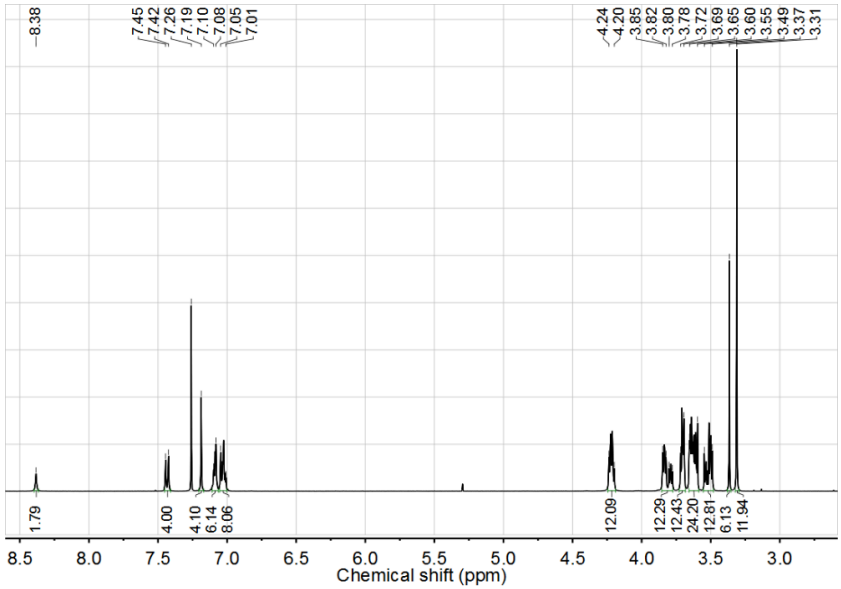

Figure S3. ^{1}H NMR spectrum of (*E*)-TPE-OEG in $CDCl_3$ (500 μL).

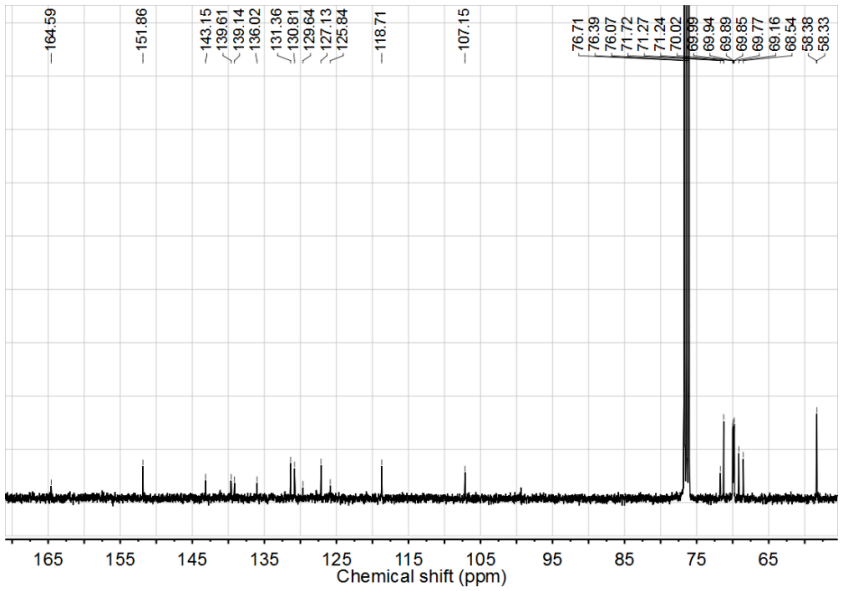

Figure S4. ^{13}C NMR spectrum of (*Z*)-TPE-OEG in $CDCl_3$ (500 μL).

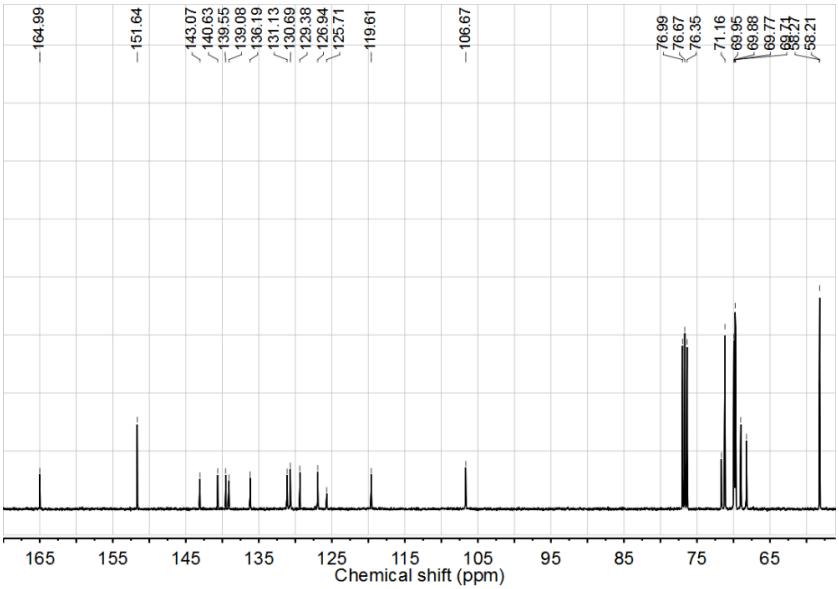

Figure S5. ^{13}C NMR spectrum of (*E*)-TPE-OEG in $CDCl_3$ (500 μL).

Figure S6. High-resolution mass spectrum of (*Z*)-TPE-OEG.

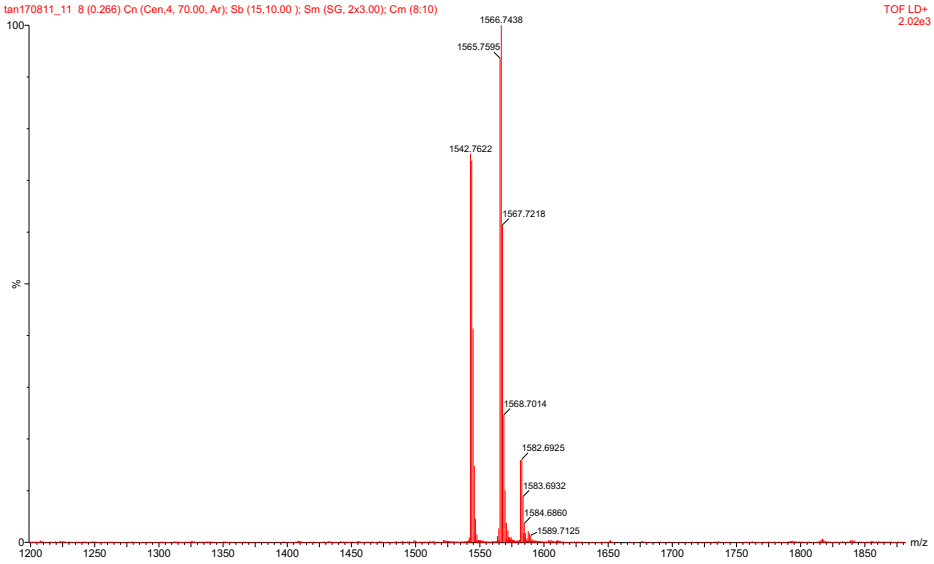

Figure S7. High-resolution mass spectrum of (*E*)-TPE-OEG.

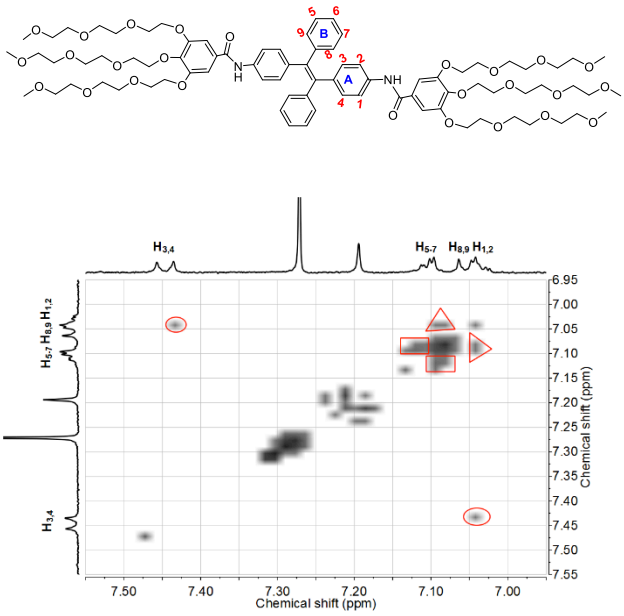

Figure S8. ^{1}H-^{1}H COSY spectrum of (*E*)-TPE-OEG.

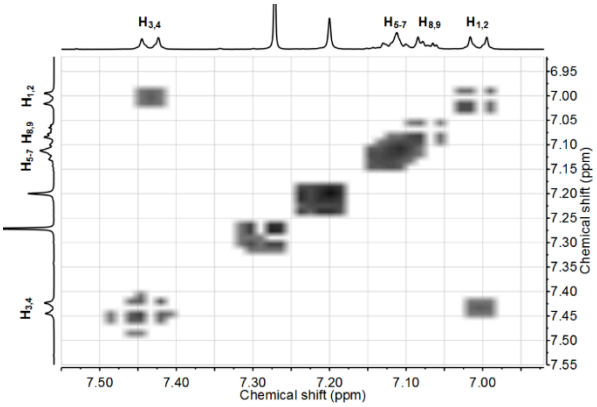

Figure S9. ^{1}H-^{1}H COSY spectrum of (*Z*)-TPE-OEG.

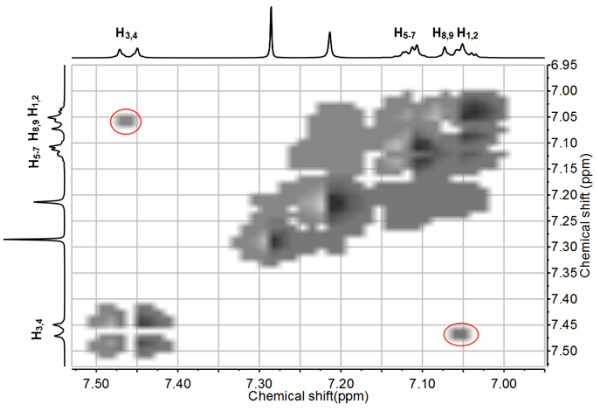

Figure S10. NOESY spectrum of (*E*)-TPE-OEG.

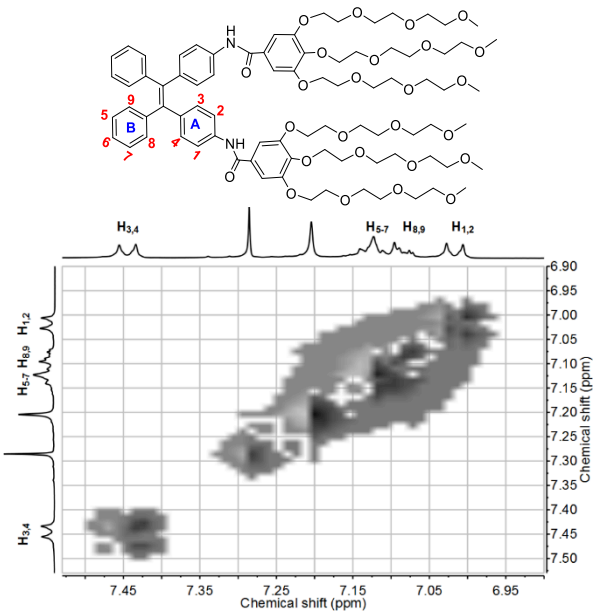

Figure S11. NOESY spectrum of (*Z*)-TPE-OEG.

3.2. Optical Properties

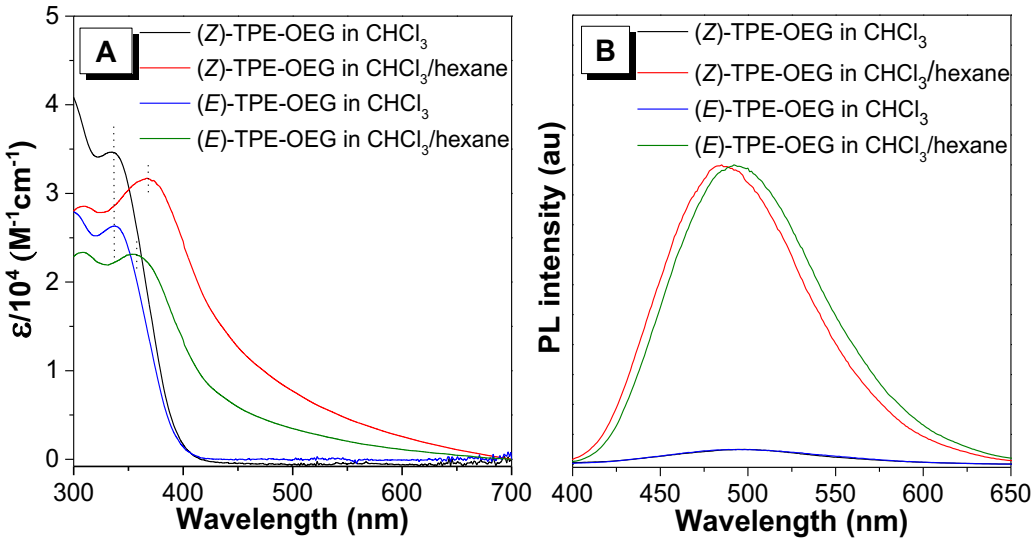

Figure S12. (A) UV and (B) normalized PL spectra of (*Z*)- and (*E*)-TPE-OEG in $CHCl_3$ and $CHCl_3$/hexane mixtures (1:99, v/v), λ_{ex} = 350 nm.

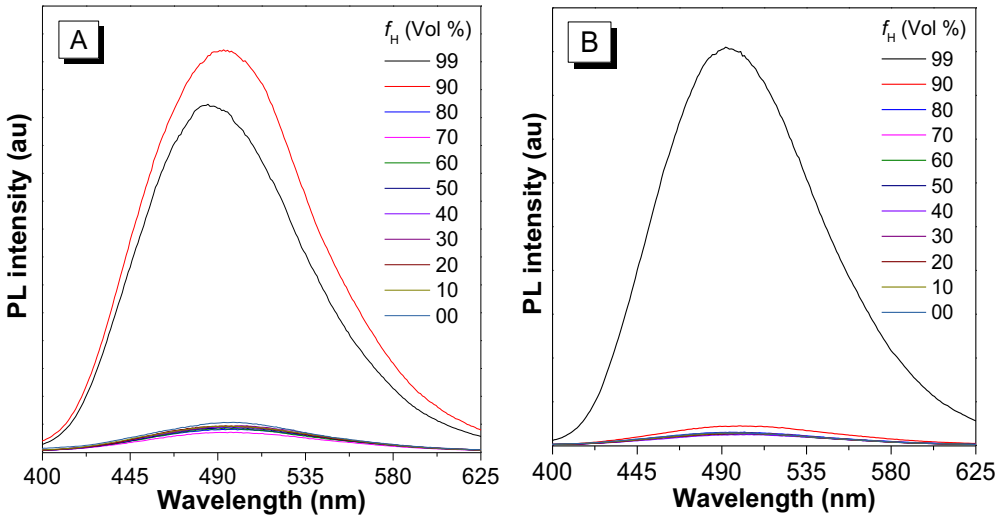

Figure S13. (A and B) PL spectra of (A) (*Z*)-TPE-OEG and (B) (*E*)-TPE-OEG in hexane/$CHCl_3$ mixtures with different hexane fractions (f_H). At high content of hexane, some large aggregate may form and precipitate, which decreased the effective dye concentration. This explains why the PL intensity of (*Z*)-TPE-OEG in 99% hexane mixture is slightly lower than that in the 90% hexane mixture.

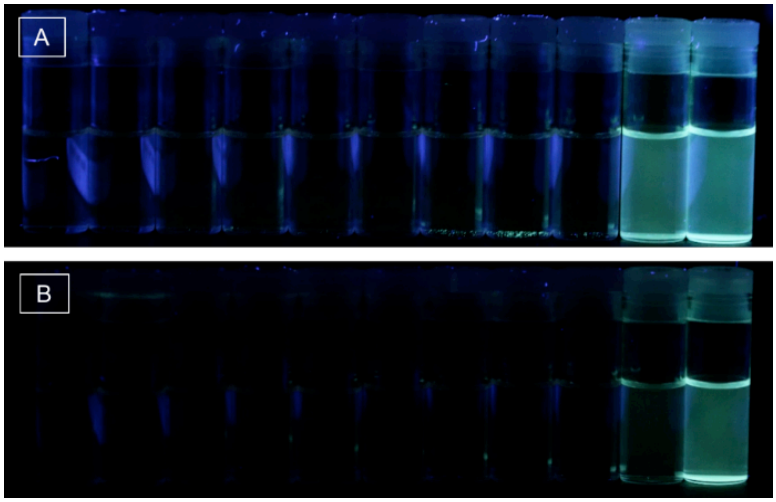

Figure S14. (A and B) Fluorescent images of (A) (*Z*)-TPE-OEG and (B) (*E*)-TPE-OEG in hexane/$CHCl_3$ mixtures with hexane fractions of 0%, 10%, 20%, 30%, 40%, 50%, 60%, 70%, 80%, 90% and 99% (from left to right).

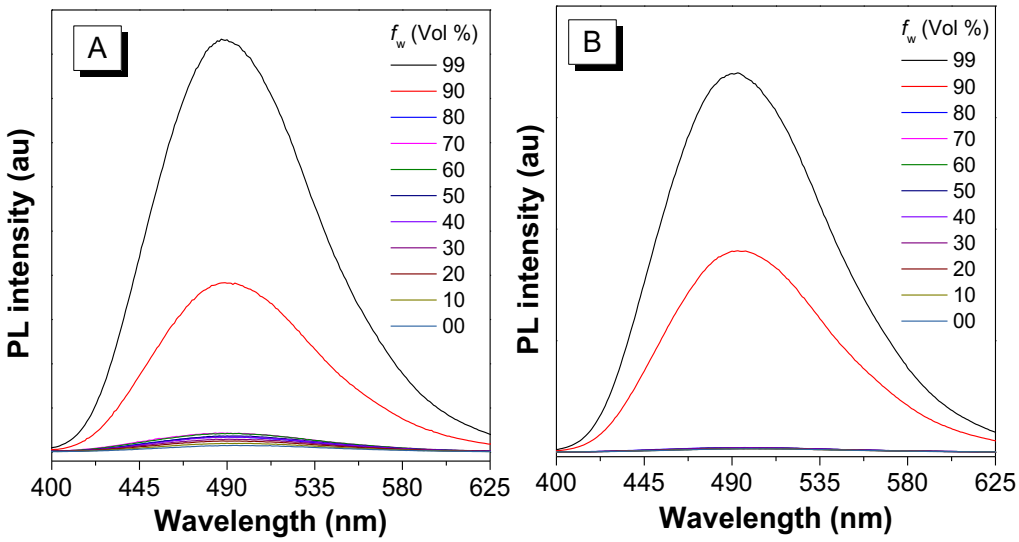

Figure S15. (A and B) PL spectra of (A) (*Z*)-TPE-OEG and (B) (*E*)-TPE-OEG in THF/water mixtures with different water fractions (f_w).

3.3. Self-Assembly Process

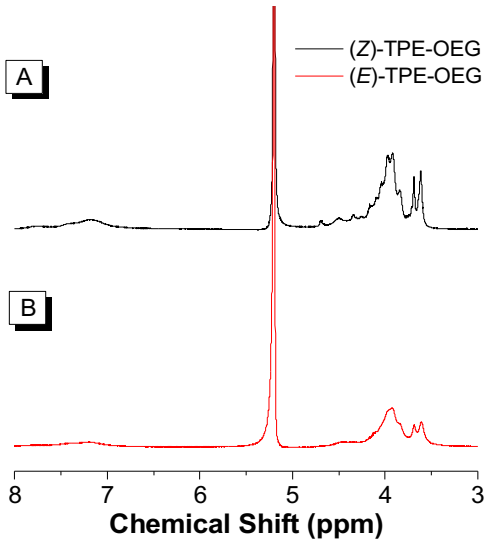

Figure S16. (A and B) ^{1}H NMR spectra of (A) (*Z*)-TPE-OEG and (B) (*E*)-TPE-OEG in D_2O (500 μL).

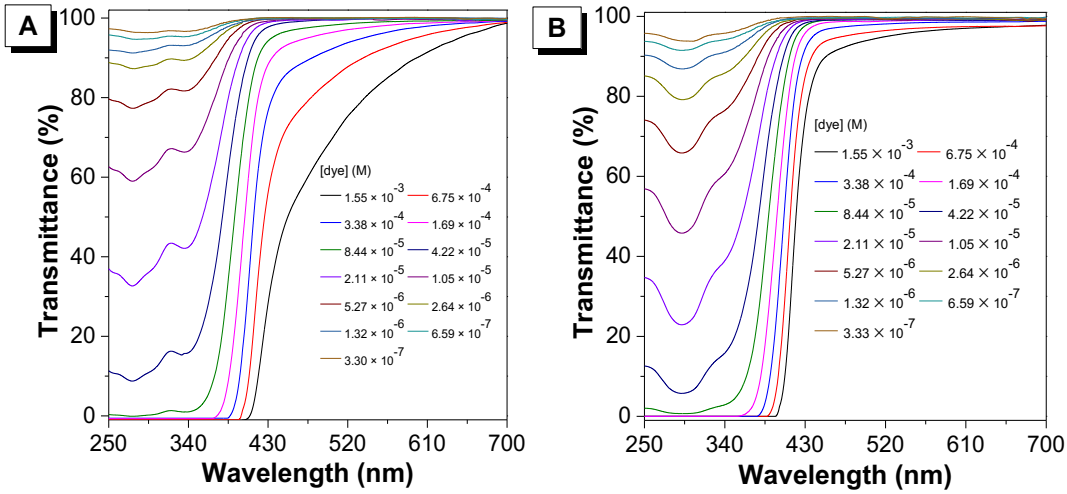

Figure S17. (A and B) Concentration-dependent optical transmittance of (A) (*Z*)-TPE-OEG and (B) (*E*)-TPE-OEG in water.

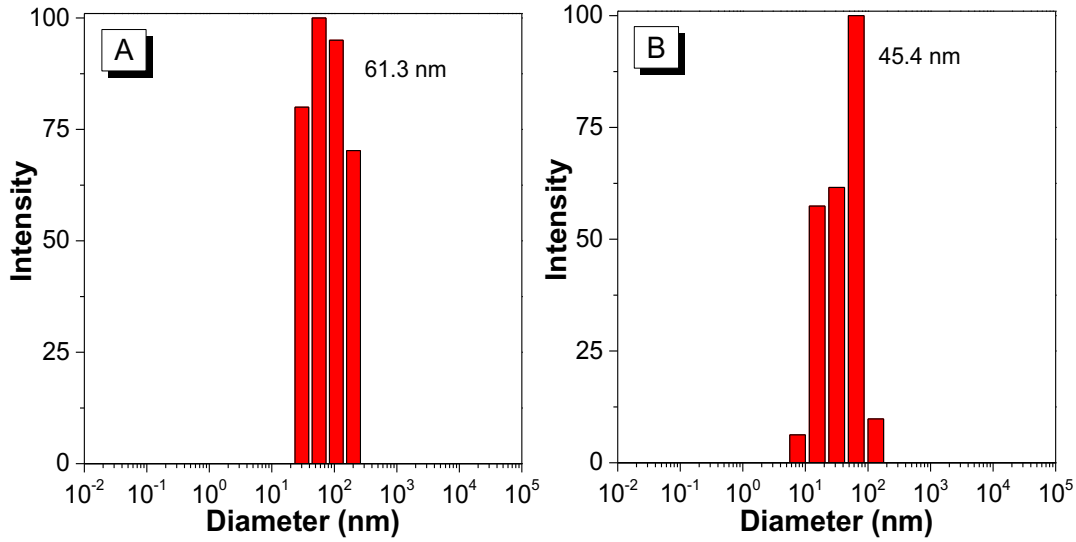

Figure S18. DLS data of the vesicles and micelles formed from (A) (*Z*)-TPE-OEG and (B) (*E*)-TPE-OEG in water. [(*Z*)-TPE-OEG] = [(*E*)-TPE-OEG] = (338 μM)

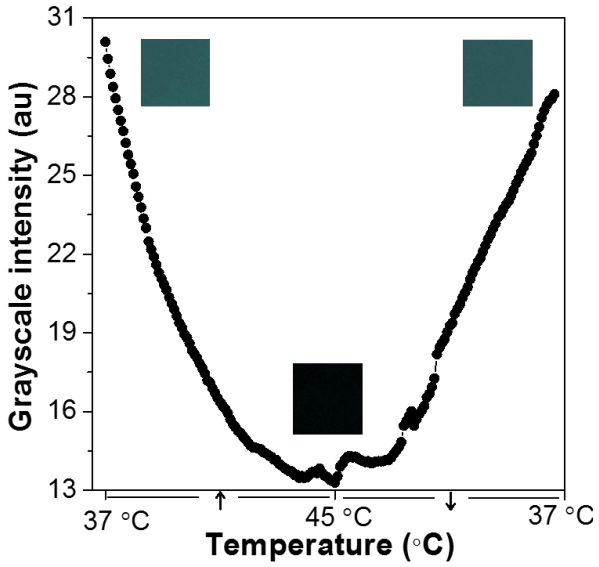

Figure S19. Plot of grayscale intensity change of CLSM images with temperature from visualization of the aqueous solution of (*Z*)-TPE-OEG (30 μM).

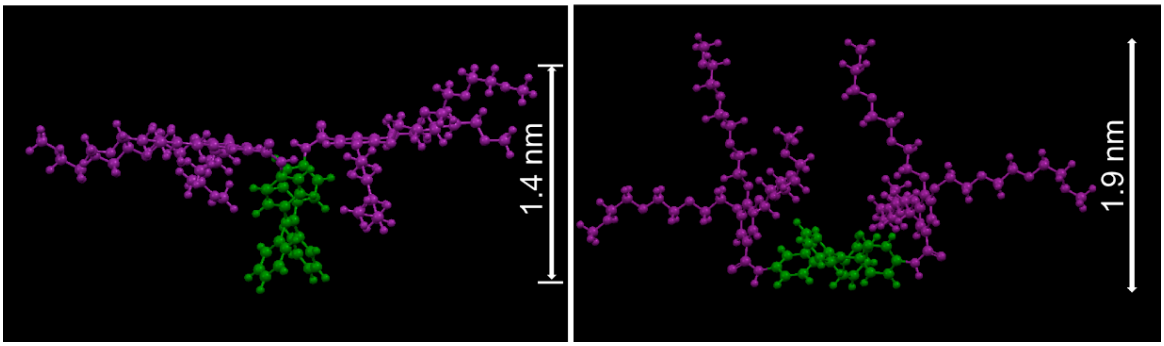

Figure S20. Optimized molecular structures of (left) (*Z*)- and (right) (*E*)-TPE-OEG in aqueous environment by Gaussian 09 program with a B3LYP/6-31G(d) method.

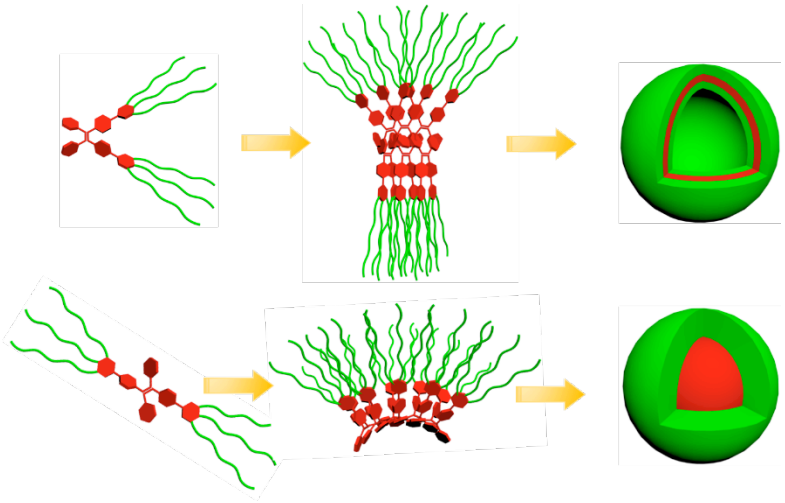

Figure S21. Self-assembly of (*Z*)-TPE-OEG and (*E*)-TPE-OEG to give vesicle and micelle in water.

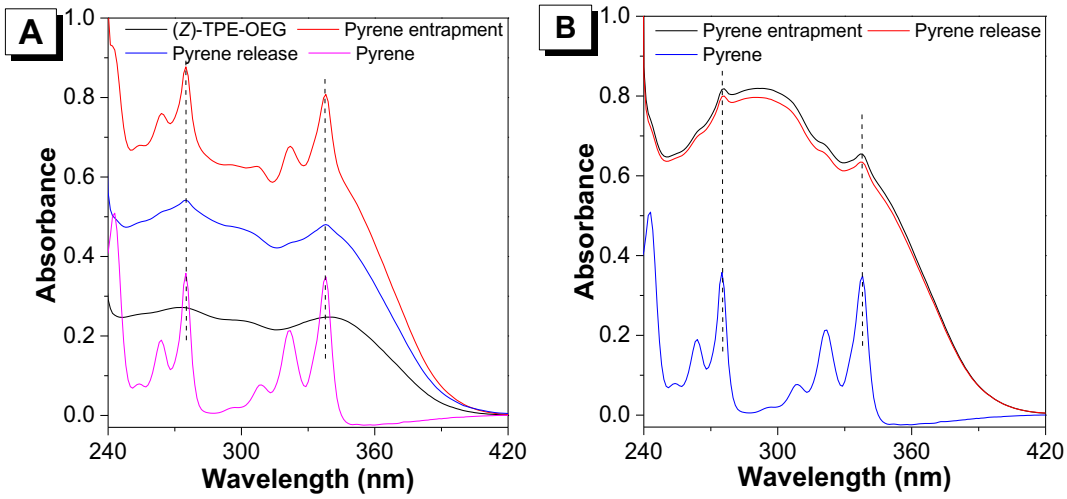

Figure S22. (A) UV spectra of pyrene (10 μM), (*Z*)-TPE-OEG (10 μM) and (*Z*)-TPE-OEG after pyrene entrapment and pyrene release. (B) UV spectra of pyrene (10 μM) and (*E*)-TPE-OEG after pyrene entrapment and pyrene release. All the samples were measured in chloroform solutions.

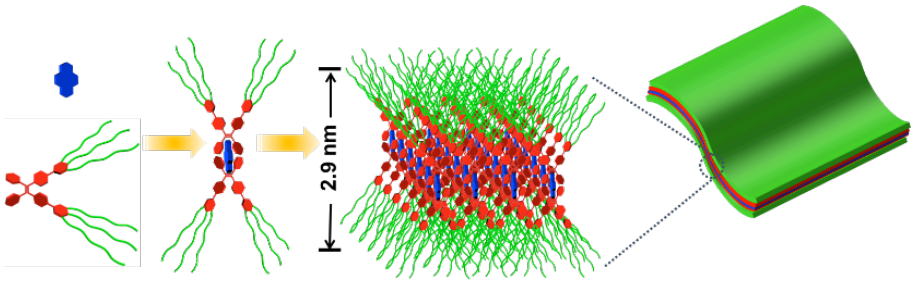

Figure S23. Schematic representation of the formation of 2D nanosheet by self-assembly of (*Z*)-TPE-OEG (3 mM) and pyrene.

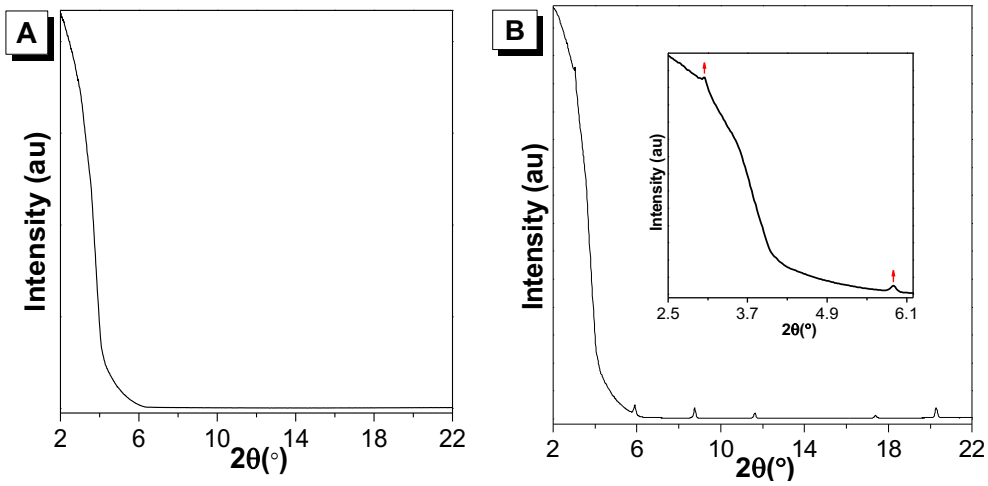

Figure S24. (A and B) XRD diffractograms of films prepared from aqueous solution of (A) (*Z*)-TPE-OEG (3 mM) and (B) (*Z*)-TPE-OEG (3 mM) entrapped with pyrene. Inset shows the partial enlarged XRD diffractogram.

3.4. Thermoresponsive Behavior

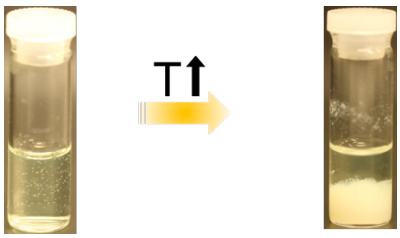

Figure S25. Pyrene release by phase transition behavior of (*Z*)-TPE-OEG. The white powder in the right bottle is the released pyrene.

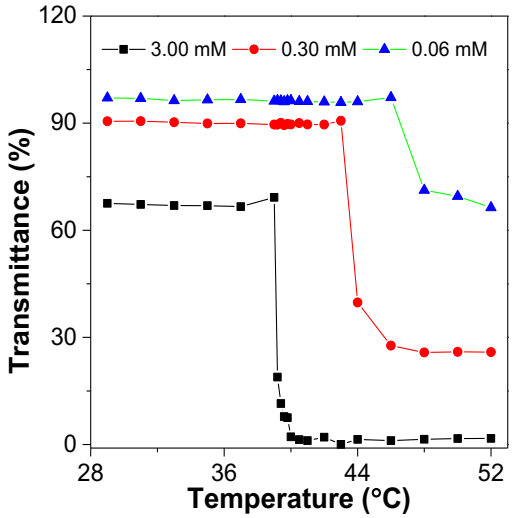

Figure S26. Plots of transmittance of (*Z*)-TPE-OEG at different concentrations in water *versus* temperature.

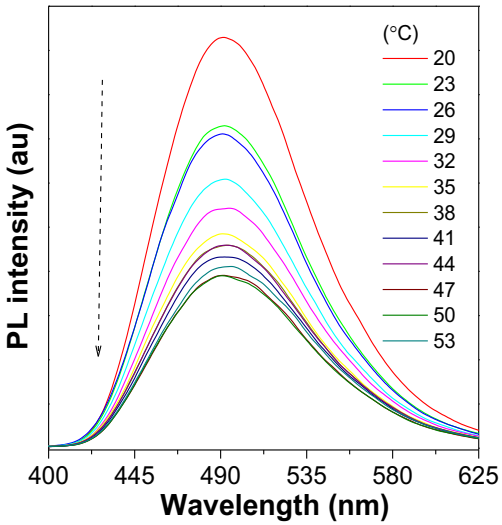

Figure S27. PL intensity changes of (*E*)-TPE-OEG in water (3 mM) in the temperature range from 20 to 53 °C.

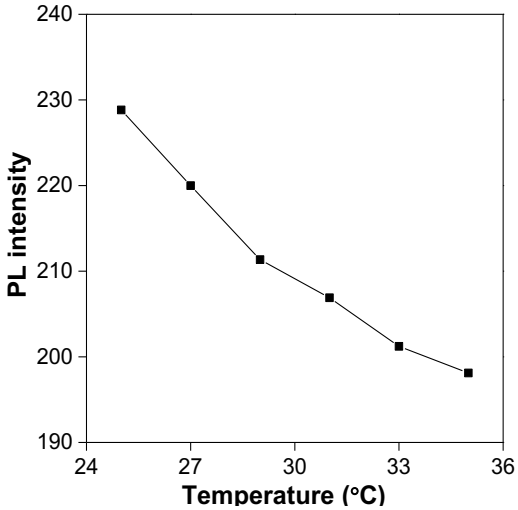

Figure S28. Temperature-dependent PL of aqueous solution (3 mM) of (*Z*)-TPE-OEG before its critical phase transition temperature.

3.5. Biological Application

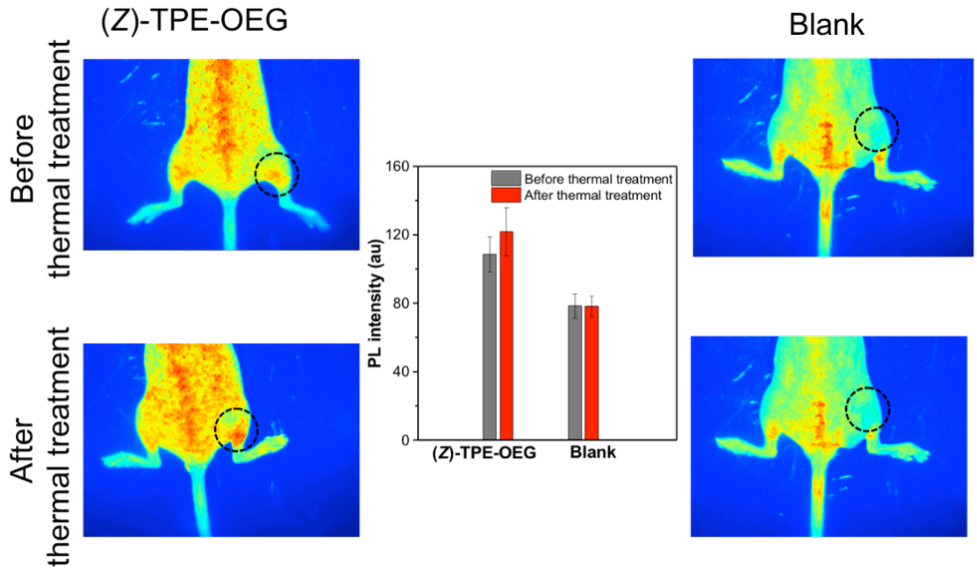

Figure S29. In vivo fluorescence imaging of nude mice after injection of (*Z*)-TPE-OEG and PBS buffer (as blank) via tail vein. The fluorescent images at a wavelength region of 500-720 nm were taken before or after the tumor sites were treated with hot pack (λ_{ex} = 455 nm).

References

[1] Peng, H.-Q.; Zheng, X.; Han, T.; Kwok, Ryan T. K.; Lam, Jacky W. Y.; Huang, X.; Tang, B. Z. Dramatic Differences in Aggregation-Induced Emission and Supramolecular Polymerizability of Tetraphenylethene-Based Stereoisomers. *J. Am. Chem. Soc.* **2017**, *139*, 10150−10156.

[2] Wang, F.; Wang, W.-G.; Wang, X.-J.; Wang, H.-Y.; Tung, C.-H.; Wu, L.-Z. A Highly Efficient Photocatalytic System for Hydrogen Production by a Robust Hydrogenase Mimic in an Aqueous Solution. *Angew. Chem. Int. Ed.* **2011**, *50*, 3193−3197.

[3] Petkau, K.; Kaeser, A.; Fischer, I.; Brunsveld, L.; Schenning, Albertus P. H. J. Pre- and Postfunctionalized Self-Assembled π-Conjugated Fluorescent Organic Nanoparticles for Dual Targeting. *J. Am. Chem. Soc.* **2011**, *133*, 17063−17071.